

# 3D magnetic configuration of the H $\alpha$ filament and X-ray sigmoid in NOAA AR 8151

S. Régnier<sup>1</sup> and T. Amari<sup>2</sup>

<sup>1</sup> Montana State University, Department of Physics, Bozeman, MT 59717, United States  
regnier@mithra.physics.montana.edu

<sup>2</sup> Centre de Physique Théorique, Ecole Polytechnique, F-91128 Palaiseau, France

Received ; accepted

**Abstract.** We investigate the structure and relationship of an H $\alpha$  filament and an X-ray sigmoid observed in active region NOAA 8151. We first examine the presence of such structures in the reconstructed 3D coronal magnetic field obtained from the non-constant- $\alpha$  force-free field hypothesis using a photospheric vector magnetogram (IVM, Mees Solar Observatory). This method allows us to identify several flux systems: a filament (height 30 Mm, aligned with the polarity inversion line (PIL), magnetic field strength at the apex 49 G, number of turns 0.5–0.6), a sigmoid (height 45 Mm, aligned with the PIL, magnetic field strength at the apex 56 G, number of turns 0.5–0.6) and a highly twisted flux tube (height 60 Mm, magnetic field strength at the apex 36 G, number of turns 1.1–1.2). By searching for magnetic dips in the configuration, we identify a filament structure which is in good agreement with the H $\alpha$  observations. We find that both filament and sigmoidal structures can be described by a long twisted flux tube with a number of turns less than 1 which means that these structures are stable against kinking. The filament and the sigmoid have similar absolute values of  $\alpha$  and  $J_z$  in the photosphere. However, the electric current density is positive in the filament and negative in the sigmoid: the filament is right-handed whereas the sigmoid is left-handed. This fact can explain the discrepancies between the handedness of magnetic clouds (twisted flux tubes ejected from the Sun) and the handedness of their solar progenitors (twisted flux bundles in the low corona). The mechanism of eruption in AR 8151 is more likely not related to the development of instability in the filament and/or the sigmoid but is associated with the existence of the highly twisted flux tube ( $\sim 1.1$ – $1.2$  turns).

**Key words.** Sun:corona – Sun:magnetic fields

## 1. Introduction

Coronal Mass Ejections (CMEs) are often related to the eruption of a filament (Webb 1988) and the existence of an S-shaped structure or sigmoid (Rust & Kumar 1996) which has been shown to be a precursor of eruptive phenomena (Canfield et al. 1999). The interplanetary consequences of CMEs are observed at 1AU as magnetic clouds. The structure of magnetic clouds has been related to the progenitor solar structures (e.g. Leamon et al. 2002): *in situ* observations of field reversal in the magnetic cloud have been interpreted as the signature of a flux rope and then related to twisted flux tubes in the low atmosphere as filament and sigmoid are often assumed to be.

Even if most of their plasma properties are known (see review by Patsourakos & Vial 2002), filaments/prominences are still under study to understand what their magnetic structure is and how they are formed. In the KS (Kippenhahn & Schlüter 1957) model, it is assumed that the filament material is supported by a mag-

netic structure containing dips (see review by Démoulin 1998). Kippenhahn & Schlüter have studied the formation of magnetic dips in a quadrupolar configuration. Note that the magnetic dips in a quadrupolar configuration appear in a "natural" way either for magnetohydrostatic equilibrium (Kippenhahn & Schlüter 1957) or for magneto-static equilibrium, namely potential and force-free fields (Amari & Aly 1989; Aly & Amari 1997). On another hand, Kuperus & Raadu (1974) have shown that magnetic dips also appear in twisted flux tubes (hereafter referred as KR model). The KS and KR models are the earliest models classifying filament structures into two different types. Many more sophisticated models were developed after KS and KR (e.g., see review by Tandberg-Hanssen 1995). Leroy et al. (1984) found that most prominences are KS-type below 30 Mm and KR-type above 30 Mm. Recently Aulanier et al. (1999) and Lionello et al. (2002) determined the filament structure by looking for the magnetic dips inside a 3D coronal magnetic configuration. Aulanier et al. (1999) have used the Low (1992) magnetohydrostatic model (*lmhs*) to determine the 3D magnetic configuration

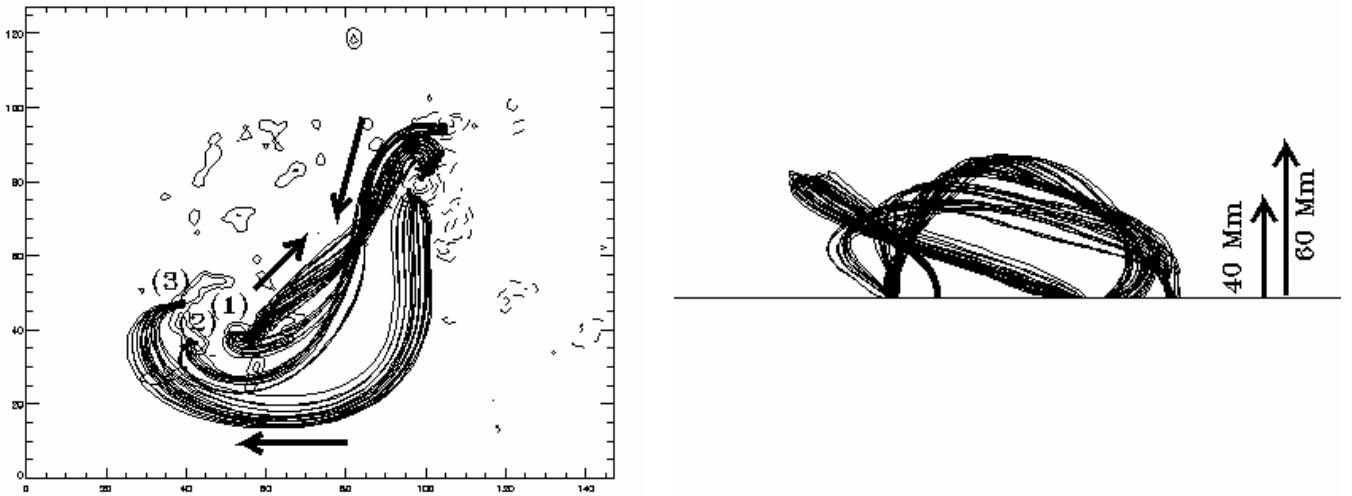


**Fig. 1.** 3D coronal magnetic configuration of AR 8151 prior to the eruption (left: top view, right: view from the West side). Three characteristic flux tubes are shown: (1) highly twisted flux tube; (2) long twisted flux tube; (3) quasi-potential flux tube. (1) and (2) match the sigmoidal structure observed in soft X-rays (Fig.3 right), and (3) matches the EUV/EIT system of loops. Arrows indicate the electric current orientation within each flux tube (from Régnier et al. 2002). On the left image, the solid (resp. dashed) contours indicate positive (resp. negative) polarities. The effective grid resolution is  $2.3''$ . North is up and West is on the right. The same computation is used throughout this paper.

in a "quiet Sun" region in which a large filament was observed. These authors have imposed a twisted flux tube in the magnetic region in order to ensure the existence of magnetic dips in the configuration which are not directly created in the *lmhs* model as well as in the linear force-free model with an  $\alpha$  value of  $0.05 \text{ Mm}^{-1}$  (Aulanier et al. 1998). Therefore, they have *a priori* assumed that the filament has a KR-type magnetic field. The authors have successfully compared the computed magnetic dips with  $H\alpha$  observations of the filament. The location of the dips are in a good agreement in both the filament (body and feet) and its channel (dark elongated fibrils). Lionello et al. (2002) have determined the filament magnetic configuration using the model developed by Amari et al. (1999b, 2000) which uses MHD boundary conditions on the photosphere. Using a line-of-sight magnetogram, the authors have built a complicated flux-rope configuration with magnetic dips as follows: (i) the initial equilibrium state is the potential field reconstructed from the line-of-sight photospheric magnetic field, (ii) the shear and twist are then developed by imposing a flow field along the neutral line (Amari et al. 1996), (iii) finally a flux cancellation process in the sheared arcade leads to the formation of the flux rope (Amari et al. 2000; Linker et al. 2001). In this KR-like configuration, the authors have found magnetic dips in a good agreement with  $H\alpha$  observations. As a result of the thermodynamic/hydrodynamic model applied to the final equilibrium (flux rope), these authors have also shown that magnetic dips can support the dense and cold material characterizing the filament material in its coronal environment. We propose here to determine the filament magnetic configuration directly from the nonlinear force-free (*nlf*) reconstructed magnetic equilibrium of an active

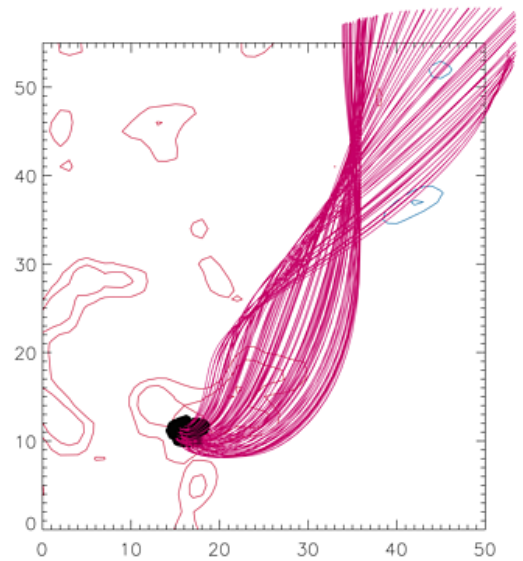


**Fig. 2.** Highly twisted flux tube referred as (1) in Fig. 1. Note that the twist is located close to the positive polarity and the electric current density is positive. See geometrical properties of the flux bundle in Table 1.

region using vector magnetogram as boundary condition, with no *a priori* assumptions on the magnetic structure (Aulanier et al. 1999) or the prior magnetic field evolution (Lionello et al. 2002). Therefore we ask this question: what kind of model (KS or KR) should we expect to describe the magnetic filament structure in an active region?

Sigmoids have been shown to be progenitors of CMEs (Canfield et al. 1999) and are often described as twisted



**Fig. 3.** Left: vertical component of the magnetic field observed by IVM surrounding by MDI magnetic field (February 11, 1998 at 17:36 UT). Center:  $H\alpha$  image (Obs. Paris-Meudon) at 08:28 UT on February 11, 1998. The filament is the dark structure. Right: soft X-ray image (SXT/Yohkoh) at 08:40 UT on February 11, 1998. The S-shaped structure is clearly observed. Both the core of the filament and the core of the sigmoid are aligned with the PIL. Those three images are co-aligned. North is up, West is on the right.

flux systems (see review by Canfield et al. 2000). The S-shaped or inverse S-shaped structures classified as sigmoids are mainly observed in soft X-ray images (SXT, Tsuneta et al. 1991) only on the solar disk. Gibson et al. (2002) have performed a complete study of a sigmoidal active region, namely AR 8668: temperature, density and velocity measurements as well as a linear force-free field extrapolation. These authors have shown that the sigmoidal structure overlaid the  $H\alpha$  filament. Recently, Leamon et al. (2003) have studied the total twist of 191 sigmoids. These authors have shown that most of the sigmoids have a total twist less than 1 turn and have concluded that although statistically sigmoids are precursors of eruptions in the corona (Canfield et al. 1999), the MHD kink instability does not trigger the eruptions. As a progenitor of CMEs, sigmoids have been related to magnetic cloud. Leamon et al. (2002) have studied the handedness of sigmoids and magnetic clouds assumed to be associated with the eruptions of the sigmoid. These authors have found that only 50% of the sigmoids and associated magnetic clouds have the same handedness. Therefore they have concluded that either the determination of the sigmoid handedness is ambiguous or that the mechanism of the sigmoid propagation into the interplanetary space is not simple (e.g. successive reconnections modify the handedness). Hence, one must ask which solar progenitors (filament and/or sigmoid) produce the magnetic cloud?

Filaments are usually observed in  $H\alpha$  and sigmoids in X-rays or hot EUV spectral lines such as FeXVI at  $360\text{\AA}$  (e.g. CDS/SOHO observations reported by Régnier et al. 1999b). Therefore how does one find the relationship between these two structures? Two approaches have recently been developed: Pevtsov (2002) has combined  $H\alpha$  and X-ray observations, and Gibson & Low (1998, 2000) have developed a model to interpret the filament-sigmoid system. Pevtsov (2002) has used 6 examples of well-observed filament-sigmoid systems to show that there is a close spatial association between the two features, which he believes to have the same topological structure.

He has concluded that both filament and sigmoid are inside a larger loop system and that no loops are between those two structures. Based on their analytic 3D MHD model, Gibson & Low (2000) have proposed two possible physical relationships between filaments and X-ray sigmoids: (i) following the model of an emerging flux rope (Matsumoto et al. 1998), the filament and the sigmoid should be coaligned with the underlying inversion line but oppositely directed (filament-sigmoid system including both S-shaped and inverse S-shaped structures), (ii) the filament and the sigmoid are the same S-shaped structure in which heating at the interface between the top of the filament and the surrounding coronal field could light up portions of the flux rope and therefore delineate the X-ray sigmoid in the same orientation as the filament. In summary, these observations and models describe the filament-sigmoid system as a system of two structures having the same topology and the same orientation. In this article, we deal with the relationship between filament and sigmoid using a different method, and reach a different conclusion.

Régnier et al. (2002, hereafter Paper I) have studied the 3D coronal magnetic field of AR 8151 using the nonlinear force-free hypothesis. In the 3D magnetic configuration (see Fig. 1), they have identified three characteristic flux tubes which match EUV (EIT/SOHO, Delaboudinière et al. 1995) and soft X-ray (SXT/Yohkoh, Tsuneta et al. 1991) images. Two of them, (1) and (2) (see Fig. 1), are twisted and highly sheared flux tubes. For the long twisted flux tube (2), the twist is estimated to 0.5–0.6 turns. The central part of this flux bundle can be associated with both the filament structure observed in  $H\alpha$  (see Fig. 3 center) and the sigmoid observed in soft X-ray (see Fig. 3 right). The other twisted flux tube (1) has  $\sim 1$ –1.2 turns. Fig. 2 shows a close-up of the highly twisted flux tube in which the non-uniform twist along the bundle is located close to the positive polarity. This twisted flux tube with a number of turns greater than  $\sim 1$  can develop a kink instability (see e.g. Hood & Priest 1981, Baty 2001 for a review

on recent progress, Amari & Luciani 1999 and Török & Kliem 2003 for 3D MHD disruption of flux ropes). From these flux tube properties, the authors (Paper I) have concluded that the eruptive phenomenon occurring in AR 8151 is likely due to the kink instability in the highly twisted flux tube and not in the less-twisted S-shaped flux tube. In their study, one key question was not tackled: what are the geometrical differences between the filament and the sigmoidal structure inferred from the nonlinear force-free magnetic configuration?

In this paper, we propose to determine characteristic parameters of the filament-sigmoid system such as location, geometry, and electric current. We will search for magnetic dips in the 3D coronal magnetic field provided by a nonlinear force-free reconstruction technique. In Section 2, we briefly summarize the observations of AR 8151 and the *nlff* field reconstruction method (more details can be found in Paper I). We then analyse the structure of the 3D coronal magnetic field (Section 3). In particular, we focus our study on finding of magnetic dips in the configuration. Quadrupolar configurations and twisted flux tubes are described. The structure of the filament and of the sigmoid are also discussed. We analyse these results in Section 4 in order to describe the relationship between the filament and the sigmoid and the implications of these structures in the eruptive phenomena associated with AR 8151.

## 2. Active region 8151 and reconstruction method

### 2.1. Active region 8151

AR 8151 was observed on February 10–15, 1998 in the South hemisphere. We focus our study on AR 8151 due to the following characteristics:

- (i) a CME observed on February 12, 1998 at 13:51 UT by EIT was determined to be propagating in the high corona as observed by LASCO C2 (Brueckner et al. 1995) at 14:27 UT with an estimated radial speed of  $540 \text{ km.s}^{-1}$  (Régnier et al. 1999a,b);
- (ii) characteristic features often defined as progenitors of CMEs are present in AR 8151, namely a filament observed in  $\text{H}\alpha$  (Fig. 3 center) and a S-shaped structure observed in soft X-ray (Fig. 3 right);
- (iii) the distribution of the vertical magnetic field on the photosphere (Fig. 3 left) looks like a dipole with a leading negative spot and a following diffuse positive polarity (and vector magnetograms are available for AR 8151 prior to the eruption).

### 2.2. Nonlinear force-free model

Although there are new techniques to measure the magnetic field into the chromosphere (Leka & Metcalf 2003) and the corona (Yurchyshyn et al. 2000; Raouafi 2000), they do not yield the 3D structure of the coronal mag-

netic field. One way to proceed is to extrapolate the photospheric magnetic field into the corona, the so-called *reconstruction problem* (Amari et al. 1997; McClymont et al. 1997, and references therein). The magnetic field in the low corona can be characterized by a plasma  $\beta$  less than 1 (e.g. Priest 1984). Therefore (neglecting the gas pressure forces) we can consider that the magnetic field configuration is in a force-free equilibrium state at a given time (expecting that the evolution time is greater than a few Alfvén times) which is a solution of:

$$\nabla \wedge \mathbf{B} = \alpha \mathbf{B} \quad (1)$$

for a force-free equilibrium,  $\mathbf{j} \wedge \mathbf{B} = \mathbf{0}$ . In Eq. 1,  $\alpha$  is 0 for the potential field,  $\alpha$  is a constant for the linear force-free (*lff*) field and  $\alpha = \alpha(\mathbf{r})$  for the nonlinear force-free (*nlff*) field. In addition, the *nlff* field should ensure that  $\alpha$  is a constant along a field line:

$$\mathbf{B} \cdot \nabla \alpha = 0. \quad (2)$$

In this paper, we use the vector potential Grad-Rubin-like method developed by Amari et al. (1997) (see also Paper I). As mentioned by Sakurai (1989), the problem is well-posed for the following boundary conditions on the photosphere: the vertical component of the magnetic field,  $B_z$  and the distribution of  $\alpha$  for a given polarity. These boundary conditions require knowledge of the full vector magnetic field on the photosphere.

### 2.3. Photospheric boundary conditions

The three components of the magnetic field are used as a photospheric boundary condition to reconstruct the coronal magnetic field. For AR 8151, the observed photospheric field is given by the IVM (Imaging Vector Magnetograph, Mickey et al. 1996). The active region was observed on February 11, 1998 at 17:36 UT. The observed field-of-view is  $280''$  square with a spatial resolution of  $1.1''$ . The time required to produce such a vector magnetogram is 3 min. The inversion of the Stokes parameters,  $I = (I, Q, U, V)$ , is performed using the so-called "weak-field" method (Jefferies et al. 1989; Jefferies & Mickey 1991). The  $180^\circ$ -ambiguity of the azimuthal component is solved using the method developed by Canfield et al. (1993). The three inverted components ( $B_{LOS}$  along the line of sight,  $B_{Trans}$  and  $B_{Azim}$  the strength and the angle of the magnetic field on the plane perpendicular to the line of sight) are transformed in the disk-center heliographic system of coordinates (Venkatakrishnan et al. 1988). To suppress edge effects due to the coordinate transformation, we reduce the IVM field-of-view to  $160'' \times 140''$ . Following Leka & Skumanich (1999), the noise level is estimated to be 50 G for the vertical component and 200 G for the transverse field. The magnetic flux through the photospheric surface is balanced.

Fig. 3 (left) is the photospheric distribution of the vertical magnetic field component  $B_z$  from the IVM observations surrounded by MDI "quiet sun" magnetic field.

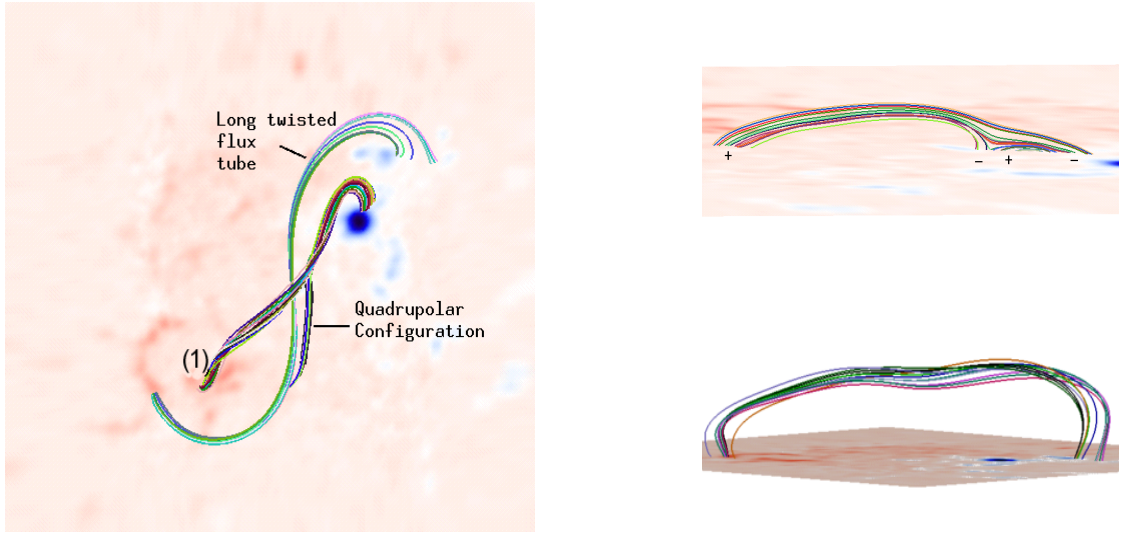


**Fig. 4.** Magnetic configurations containing magnetic dips. Left: top view of the quadrupolar configuration and the long twisted flux tube (the flux tube (1) is included as a reference). Top right: view from the right side of the quadrupolar configuration (smaller scale than the top view); Bottom right: view from the right side of the long twisted flux tube. See text for details.

We add this surrounding magnetic field to take into account some small polarities outside the IVM field-of-view and also to confine the active region magnetic field by the surrounding potential field.

From the three components in cartesian coordinates,  $(B_x, B_y, B_z)$ , we derive the vertical electric current density,

$$J_z = \frac{1}{\mu_0} \left( \frac{\partial B_y}{\partial x} - \frac{\partial B_x}{\partial y} \right), \quad (3)$$

and the  $\alpha$  distribution,

$$\alpha = \frac{J_z}{B_z}. \quad (4)$$

Note that to compute those two photospheric quantities we consider only values of the magnetic field greater than the noise levels given above. The  $\alpha$  distribution ranges between  $-1 \text{ Mm}^{-1}$  and  $1 \text{ Mm}^{-1}$  which contains high  $\alpha$  values compared to averaged or best  $\alpha$  values,  $\sim 10^{-2} \text{ Mm}^{-1}$  (Leka & Skumanich 1999).

To summarize, the photospheric boundary conditions are provided by the measurement of the full vector magnetic field on the photosphere: the vertical component of the magnetic field,  $B_z$  and the distribution of  $\alpha$  derived from the transverse components.

### 3. Filament and sigmoidal structure

#### 3.1. Finding magnetic dips

In this Section, we present the method that we use to find and classify magnetic dips in the 3D configuration.

To locate the magnetic dips in the 3D coronal magnetic configuration, we have to search for significant changes of curvature along a field line characterizing a minimum (the

tangent to the curve is almost horizontal and the derivative becomes positive). Let us define the three vectors of the Frenet frame for the curve by the right handed triplet  $(\mathcal{T}, \mathcal{N}, \mathcal{B})$ :  $\mathcal{T}$  is the tangent to the curve,  $\mathcal{N}$  is the normal vector,  $\mathcal{B}$  is the binormal vector such as  $\mathcal{B} = \mathcal{T} \wedge \mathcal{N}$ . The coordinate along the field line is  $s$ . We have the following relation:

$$\frac{d\mathcal{T}}{ds} = c\mathcal{N} \quad (5)$$

where  $c$  is the curvature of the field line.  $R = \frac{1}{c}$  is the radius of the osculating circle  $\mathcal{C}$  at a given point  $\mathcal{M}$  of the curve. The center of this circle gives us the concavity of the field line which allows us to define the magnetic dips: if  $\mathcal{M}$  is a minimum of the curve and if the centre of  $\mathcal{C}$  is upper than the curve (concave upward region) then  $\mathcal{M}$  is considered to be a magnetic dip. Practically, we first plot a field line defined as follows:

$$\frac{dx}{B_x} = \frac{dy}{B_y} = \frac{dz}{B_z} = \frac{ds}{B}. \quad (6)$$

From Eqns. (5) and (6), we define the relation between the magnetic field and the curvature of magnetic field lines in 3D:

$$c \mathcal{N} = \frac{1}{B^2} (\mathbf{B} \cdot \nabla) \mathbf{B} - \frac{\mathbf{B}}{B^3} \mathbf{B} \cdot \nabla B, \quad (7)$$

and then we estimate the curvature  $c$  and the location of the center of  $\mathcal{C}$ .

#### 3.2. 3D magnetic structure of the filament and the sigmoid

We use the above method to locate all magnetic dips in the 3D magnetic configuration of AR 8151. As expected, we find two types of dips: dips appearing because



**Fig. 5.** Left: magnetic dipoles in quadrupolar configurations (top view) which do not match the location of the observed filament; center:  $H\alpha$  image of the filament in AR 8151; right: magnetic dipoles in long twisted flux tube (top view) which match the core of the observed filament.

of the quadrupolar configuration (Fig. 4 top right) and dipoles along a twisted flux tube (Fig. 4 bottom right). In Fig. 4, we plot the field lines (or flux tubes) associated with the magnetic dipoles. Fig. 4 left is a top view of the quadrupolar configuration and the long twisted flux tubes (as annotated on the figure). For the sake of comparison, the highly twisted flux tube (1) (see Fig. 1) is also plotted. Fig. 4 top right is a side view of the quadrupolar configuration (the polarities are mentioned on the figure); it is an asymmetric quadrupolar distribution, the height is estimated to be 15 Mm. Fig. 4 bottom right is a side view of the long twisted flux tube exhibiting magnetic dipoles: the height is estimated to be 34 Mm. Note that with the *nlf* field reconstruction method we are able to obtain both types of configurations, namely KS (quadrupolar) and KR (flux rope) configurations with magnetic dipoles. The long twisted flux tube has a magnetic structure which can be compared to the theoretical model of helical field in the pre-eruptive stage (Antiochos et al. 1994; DeVore & Antiochos 2000).

In Fig. 5, we plot the magnetic field lines containing dipoles from the location of the dip to footpoints (not the entire field line is plotted). The magnetic dip distributions are shown for the quadrupolar configurations (Fig. 5 left) and for the long twisted flux tube (Fig. 5 right). On one hand, the distribution of magnetic dipoles in quadrupolar configurations is localized in few parts of the active region. On the other hand, the distribution of magnetic dipoles in the twisted flux tube is approximately located along the PIL. By comparing these two distributions and the  $H\alpha$  image (Fig. 5 center), it is obvious that the filament is well described by the magnetic dipoles along the twisted flux tube. Therefore we identify the filament magnetic structure as the long twisted flux tube as shown in Fig. 4 and the sigmoid magnetic structure as the undipped twisted flux tube (2) as shown in Fig. 1 (see also Paper I). A schematic depiction of the filament and the sigmoid (both of them characterised by a single field line) is given in Fig. 6.

In Table 1, we summarize the characteristic parameters of the flux tubes identified as the filament and the

sigmoid. In addition we provide the same parameters for the quasi-potential flux system (3) and the highly twisted flux tube (1) (see Paper I and Fig. 1). From the photospheric parameters, we note that the vertical electric current density as well as the  $\alpha$  value (see Eq. (4)) in the filament and in the sigmoid are similar in absolute value but are opposite in sign.  $J_z$  and  $\alpha$  values are small in the quasi-potential flux tube. In the highly twisted flux tube, the  $\alpha$  value is small ( $0.03 \text{ Mm}^{-1}$ ). Nevertheless,  $J_z$  is high due to the high magnetic field strength at the footpoint of 1300 G instead of 200 G for the filament and the sigmoid. The  $\alpha$  value for the filament and the sigmoid is  $\sim 100$  times higher than the  $\alpha_{best}$  value of the whole active region on the photosphere ( $|\alpha_{best}| = 2.6 \cdot 10^{-3} \text{ Mm}^{-1}$ , Régnier et al. 1999b). From the 3D magnetic field, we derive geometrical parameters as well as magnetic properties of each flux tube: the length  $L$ , the height  $h$ , the magnetic field strength at the top of the loop  $B_h$ . The comparison of  $L$ ,  $h$  and  $\pi d$  (length of the loop as a semi-circular loop) indicates how far the flux tubes are from the potential field in terms of curvature: the filament and the sigmoid have a huge discrepancy from the potential field. The differences between these field lines and the potential field are also given by the shear angle  $\frac{\pi}{2} - \theta_s$  where  $\theta_s$  is defined as the angle between the PIL and the projection of a field line onto the photospheric plane. The filament and the sigmoid are almost aligned with the PIL (high shear angle). The shear angle for the quasi-potential flux tube is also high ( $\sim 40^\circ$ ). This definition does not take into account the evolution of the neutral line with height. The closest to a potential configuration in terms of shear angle and curvature is the highly twisted flux tube. One other parameter derived from the magnetic configuration is the magnetic field strength at the summit of the loop system,  $B_h$ . For the filament,  $B_h$  is  $\sim 50$  G in agreement with the measurements of active region filament magnetic fields reported by Tandberg-Hanssen (1995). We also report the results given by the search of magnetic dipoles in the 3D coronal magnetic configuration:  $N$  the number of

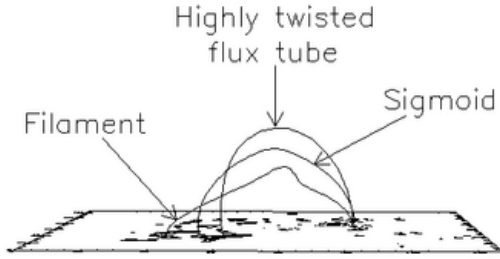


**Fig. 6.** Schematic drawing of the filament and sigmoid system: one field line is used to describe the location and the geometry of both structures.

turns (see Paper I) and the existence of magnetic dips in the flux bundle. Only the filament structure contains dips.

From Table 1, we also derive the aspect ratio defined as  $\frac{2h}{d}$ . Following the classification of loops by Magara & Longcope (2003), the filament and the sigmoid have an aspect ratio less than 1 and therefore can be classified as undulating field lines which characterize the inner field lines of an emerging flux tube. Those inner field lines are aligned with the neutral line and often contain magnetic dips. The highly twisted flux tube and the quasi-potential flux bundle have an aspect ratio greater than 1. These field lines characterize the outer field lines of the emerging flux tube and they are mostly unshredded arcades.

In Amari et al. (1999a), the vector potential Grad-Rubin reconstruction method was applied to exact known solutions (Low 1982; Low & Lou 1990) in order to estimate the errors comparing reconstructed and exact magnetic fields. These authors have shown that the errors are never more than a few percent, except near the lateral and top boundaries where the condition  $\mathbf{B} \cdot \mathbf{n} = 0$  is imposed. Therefore the main source of errors in the reconstruction process is due to the boundary condition on the photosphere. First, errors are associated with the inversion procedure of the Stokes parameters (see discussion in Klimchuk et al. 1992). The main errors are due to the resolution of the  $180^\circ$  ambiguity existing on the transverse components. These errors cannot be quantified because we do not know *a priori* the exact solution, especially along the PIL. Another source of error is the noise on the measured magnetic field components. The analysis of these errors is made following Leka & Skumanich (1999) (see Section 2). Considering the virial theorem (Klimchuk et al. 1992; Bleybel et al. 2002), we consider that the errors on the magnetic energy are not greater than 20%. These relative errors do not weaken our conclusions on the magnetic nature of the filament and the sigmoid (see Table 1).

#### 4. Discussion and conclusions

We have applied the vector potential Grad-rubin reconstruction method to determine the 3D *nlf* magnetic field of active region AR 8151. We have focused our study on

**Table 1.** Characteristic parameters for the filament and the sigmoid, the quasi potential and the highly twisted flux tubes: photospheric parameters ( $d$  length between the footpoints of the flux bundle,  $\alpha$ ,  $J_z$  the vertical current density), geometrical parameters of the flux systems inferred from the reconstructed 3D magnetic field ( $L$  length,  $h$  height,  $\theta_s$  shear angle,  $B_h$  magnetic field strength at the top of the field lines),  $N$  number of turns, and the existence of magnetic dips and the aspect ratio are also reported.

	Filament	Sigmoid	Quasi-potential (3)	Highly twisted (1)
$d$ (Mm)	130	125	98	85
$\alpha$ ( $\text{Mm}^{-1}$ )	0.15	-0.15	$-6 \cdot 10^{-3}$	0.03
$J_z$ ( $\text{mA} \cdot \text{m}^{-2}$ )	2.4	-2.3	-0.7	3.5
$L$ (Mm)	205	180	220	169
$h$ (Mm)	34	45	54	61
$\theta_s$	$5^\circ$	$5^\circ$	$50^\circ$	$75^\circ$
$B_h$ (G)	49	56	20	36
$N$	0.5–0.6		0	1.1–1.2
Magnetic Dips	Yes	No	No	No
Aspect Ratio	0.52	0.72	1.1	1.44

the system of twisted flux tubes associated with a filament and a sigmoid. We can summarize our findings as follows:

- Global structure of AR 8151:
  - (i) with the *nlf* reconstruction method, we obtain the 3D coronal magnetic configuration of an active region with a large range of  $\alpha$  values. This allows us to have structures with high shear and/or with high twist and/or with a potential-like configuration;
  - (ii) we are able to identify the magnetic dips in the 3D configuration. We obtain the two types of dipped structures: the KS and the KR configurations.
- Filament-sigmoid system
  - (i) both the filament and the sigmoid are described by long twisted flux tubes;
  - (ii) the filament contains magnetic dips and the sigmoid does not. The filament dips are located at the center of the structure or at the top of the flux bundle which means that the twist is uniformly distributed in the filament. For the sigmoid and the highly twisted flux tube, the twist is not uniformly distributed along the magnetic structures which explain that no magnetic dips are found;
  - (iii) the  $\alpha$  value and the current density  $J_z$  associated with the filament are opposite in sign to the ones in the sigmoid;

- (iv) the sigmoid is higher in the corona than the filament;
- (v) in both structures, the twist (number of turns,  $N$ ) is smaller than 1. That is to say, these structures are stable against kinking.

Our results are in agreement with the observations detailed in Pevtsov (2002) and with the model described by Gibson & Low (2000): the sigmoid is higher than the filament in the corona and the filament and the sigmoid have the same orientation. In addition to that, we are able to characterize the electric current density in these structures and to conclude that the current is opposite in the filament and in the sigmoid. Note that the relative magnetic helicity of the *nlf* field is

$$\Delta H_m = 4.7 \cdot 10^{41} Mx^2 \quad (8)$$

(corrected value from Régnier et al. 2002) where  $\Delta H_m$  is given by (Berger & Field 1984):

$$\Delta H_m = \int_{\Omega} (\mathbf{A} - \mathbf{A}_0) \cdot (\mathbf{B} + \mathbf{B}_0) d^3r \quad (9)$$

when the boundary conditions,  $\mathbf{B} \cdot \mathbf{n} = 0$  are applied on the sides of the computational box other than the photosphere. Note that with these boundary conditions, the Berger & Field formula gives the same value of relative magnetic helicity as the Finn & Antonsen (1985) formula. The positive sign of the relative magnetic helicity is in agreement with the chirality rules (Pevtsov et al. 1995; Longcope et al. 1998) for an active region located in the South hemisphere as AR 8151. The sign of  $\Delta H_m$  is the same as the sign of the  $\alpha$  values associated with the filament and the highly twisted flux tube.

We have no data showing evidence of a magnetic cloud associated with the eruption occurring in AR 8151. Nevertheless, we have shown that in the same active region we can have structures with the same orientation (S-shaped filament and sigmoid) but a different handedness. This fact can explain the discrepancies obtained by Leamon et al. (2002) by comparing sigmoids and magnetic cloud handedness: both left-handed and right-handed structures are present in the reconstructed configuration of AR 8151.

We have shown that the filament and the sigmoid are stable structures in terms of kink instability. Therefore, if we assume no dramatic evolution of these structures before the eruption ( $\sim 20$  hours between the snapshot studied here and the eruption), the filament and the sigmoid have no active role in this phenomena. Only the highly twisted flux tube is likely to erupt and then to be related to the magnetic cloud (unfortunately no evidence of magnetic cloud is shown in the *in situ* measurements).

Even if the filament-sigmoid system is well described for AR 8151 by our study, we now need to understand how the stability of these structures can evolve prior to the eruptive event. Moreover some points still remain unclear: Is the filament-sigmoid system a single current system (or closed current circuit)? How the heating and/or cooling

take place in this system which can explain the formation and the evolution of these magnetic structures?

*Acknowledgements.* We are really grateful to R. C. Canfield for his willingness to referee this paper at different stages of the writeup process. This work is supported by AFOSR, under a DoD Multi-Universities Research Initiative (MURI) grant. We thank the Berkeley MURI team for fruitful discussions and the CNES (Centre National des Études Spatiales) for its support. This work will continue as a part of the European Solar Magnetism Network (EC contract HPRN-CT-2002-00313).

## References

- Aly, J. J. & Amari, T. 1997, *A&A*, 319, 699  
 Amari, T. & Aly, J. J. 1989, *A&A*, 208, 261  
 Amari, T., Aly, J. J., Luciani, J. F., Boulmezaoud, T. Z., & Mikic, Z. 1997, *Solar Phys.*, 174, 129  
 Amari, T., Boulmezaoud, T. Z., & Mikic, Z. 1999a, *A&A*, 350, 1051  
 Amari, T. & Luciani, J. F. 1999, *ApJ*, 515, L81  
 Amari, T., Luciani, J. F., Aly, J. J., & Tagger, M. 1996, *ApJ*, 466, L39  
 Amari, T., Luciani, J. F., Mikic, Z., & Linker, J. 1999b, *ApJ*, 518, L57  
 Amari, T., Luciani, J. F., Mikic, Z., & Linker, J. 2000, *ApJ*, 529, L49  
 Antiochos, S. K., Dahlburg, R. B., & Klimchuk, J. A. 1994, *ApJ*, 420, L41  
 Aulanier, G., Démoulin, P., Mein, N., et al. 1999, *A&A*, 342, 867  
 Aulanier, G., Démoulin, P., van Driel-Gesztelyi, L., Mein, P., & Deforest, C. 1998, *A&A*, 335, 309  
 Baty, H. 2001, *A&A*, 367, 321  
 Berger, M. A. & Field, G. B. 1984, *Journal of Fluid Mechanics*, 147, 133  
 Bleybel, A., Amari, T., van Driel-Gesztelyi, L., & Leka, K. D. 2002, *A&A*, 395, 685  
 Brueckner, G. E., Howard, R. A., Koomen, M. J., et al. 1995, *Solar Phys.*, 162, 357  
 Canfield, R. C., de La Beaujardière, J.-F., Fan, Y., et al. 1993, *ApJ*, 411, 362  
 Canfield, R. C., Hudson, H. S., & McKenzie, D. E. 1999, *Geophys. Res. Lett.*, 26, 627  
 Canfield, R. C., Hudson, H. S., & Pevtsov, A. A. 2000, *IEEE Transactions On Plasma Science, Special Issue on Space Plasmas*, 1786  
 Delaboudinière, J.-P., Artzner, G. E., Brunaud, J., et al. 1995, *Solar Phys.*, 162, 291  
 Démoulin, P. 1998, in *ASP Conf. Ser. 150: IAU Colloq. 167: New Perspectives on Solar Prominences*, 78  
 DeVore, C. R. & Antiochos, S. K. 2000, *ApJ*, 539, 954  
 Finn, J. M. & Antonsen, T. M. 1985, *Comments Plasma Phys. Controlled Fusion*, 9, 111  
 Gibson, S. E., Fletcher, L., Del Zanna, G., et al. 2002, *ApJ*, 574, 1021  
 Gibson, S. E. & Low, B. C. 1998, *ApJ*, 493, 460  
 Gibson, S. E. & Low, B. C. 2000, *J. Geophys. Res.*, 105, 18187

- Hood, A. W. & Priest, E. R. 1981, *Geophysical and Astrophysical Fluid Dynamics*, 17, 297
- Jefferies, J., Lites, B. W., & Skumanich, A. 1989, *ApJ*, 343, 920
- Jefferies, J. T. & Mickey, D. L. 1991, *ApJ*, 372, 694
- Kippenhahn, R. & Schlüter, A. 1957, *Zeitschrift Astrophysics*, 43, 36
- Klimchuk, J. A., Canfield, R. C., & Rhoads, J. E. 1992, *ApJ*, 385, 327
- Kuperus, M. & Raadu, M. A. 1974, *A&A*, 31, 189
- Leamon, R. J., Canfield, R. C., Blehm, Z., & Pevtsov, A. A. 2003, *ApJ*, 596, L255
- Leamon, R. J., Canfield, R. C., & Pevtsov, A. A. 2002, in *Journal of Geophysical Research (Space Physics)*, Volume 107, Issue A9, 1–1
- Leka, K. D. & Metcalf, T. R. 2003, *Solar Phys.*, 212, 361
- Leka, K. D. & Skumanich, A. 1999, *Solar Phys.*, 188, 3
- Leroy, J. L., Bommier, V., & Sahal-Brechot, S. 1984, *A&A*, 131, 33
- Linker, J. A., Lionello, R., Mikić, Z., & Amari, T. 2001, *J. Geophys. Res.*, 106, 25165
- Lionello, R., Mikić, Z., Linker, J. A., & Amari, T. 2002, *ApJ*, 581, 718
- Longcope, D. W., Fisher, G. H., & Pevtsov, A. A. 1998, *ApJ*, 507, 417
- Low, B. C. 1982, *Solar Phys.*, 77, 43
- Low, B. C. 1992, *ApJ*, 399, 300
- Low, B. C. & Lou, Y. Q. 1990, *ApJ*, 352, 343
- Magara, T. & Longcope, D. W. 2003, *ApJ*, 586, 630
- Matsumoto, R., Tajima, T., Chou, W., Okubo, A., & Shibata, K. 1998, *ApJ*, 493, L43
- McClymont, A. N., Jiao, L., & Mikic, Z. 1997, *Solar Phys.*, 174, 191
- Mickey, D. L., Canfield, R. C., Labonte, B. J., et al. 1996, *Solar Phys.*, 168, 229
- Patsourakos, S. & Vial, J. 2002, *Solar Phys.*, 208, 253
- Pevtsov, A. A. 2002, *Solar Phys.*, 207, 111
- Pevtsov, A. A., Canfield, R. C., & Metcalf, T. R. 1995, *ApJ*, 440, L109
- Priest, E. R. 1984, *Solar magneto-hydrodynamics (Geophysics and Astrophysics Monographs, Dordrecht: Reidel)*
- Raouafi, N.-E. 2000, PhD Thesis
- Régnier, S., Amari, T., & Kersalé, E. 2002, *A&A*, 392, 1119
- Régnier, S., Amari, T., Solomon, J., Vial, J.-C., & Mickey, D. 1999a, in *8th SOHO Workshop: Plasma Dynamics and Diagnostics in the Solar Transition Region and Corona*, ESA SP Series (SP-446), eds. J.C. Vial & B. Kaldeich-Schürmann, 571
- Régnier, S., Solomon, J., Vial, J.-C., Amari, T., & Mickey, D. 1999b, in *Ninth European Meeting on Solar Physics: Magnetic Fields and Solar Processes*, ESA SP Series (SP-448), ed. A. Wilson., 519
- Rust, D. M. & Kumar, A. 1996, *ApJ*, 464, L199
- Sakurai, T. 1989, *Space Science Reviews*, 51, 11
- Török, T. & Kliem, B. 2003, *A&A*, 406, 1043
- Tandberg-Hanssen, E. 1995, *The nature of solar prominences (Astrophysics and Space Science Library, vol. 199, Dordrecht: Kluwer Academic Publishers)*
- Tsuneta, S., Acton, L., Bruner, M., et al. 1991, *Solar Phys.*, 136, 37
- Venkatakrishnan, P., Hagyard, M. J., & Hathaway, D. H. 1988, *Solar Phys.*, 115, 125
- Webb, D. F. 1988, *J. Geophys. Res.*, 93, 1749
- Yurchyshyn, V. B., Wang, H., Qiu, J., Goode, P. R., & Abramenko, V. I. 2000, *ApJ*, 1143